# Goal-Oriented Time-Series Forecasting: Foundation Framework Design

Luca-Andrei Fechete[*†] Mohamed Sana[†] Fadhel Ayed[†] Nicola Piovesan[†]
Wenjie Li[†] Antonio De Domenico[†] Tareq Si Salem[†‡]

## Abstract

Conventional forecasting minimizes overall error but overlooks the differing importance of forecast ranges in downstream tasks. We propose a method that partitions predictions into segments and dynamically reweights them at inference, enabling flexible, on-demand targeted forecasting without retraining. Experiments on benchmarks and a new wireless dataset show improved accuracy in regions of interest and measurable downstream gains, highlighting the benefits of tighter integration between prediction and decision-making.

## 1 Introduction

Time-series forecasting (TSF) is a core area of machine learning (ML) with applications in economics (Granger and Newbold, 2014), energy (Martín et al., 2010; Qian et al., 2019), transportation (Chen et al., 2001), meteorology (Wu et al., 2023), inventory management (Li et al., 2022), and healthcare (Ghassemi et al., 2015; Ray et al., 2025). At its core, TSF builds predictive models for sequential data by leveraging historical patterns to forecast future values. Approaches range from classical statistical models, such as ARIMA (Hyndman and Athanasopoulos, 2015) and ETS (Brown, 1956), to deep learning models, including MLPs (Zeng et al., 2023), RNNs (Zhang and Man, 1998), LSTMs (Siami-Namini et al., 2019), TCNs (He and Zhao, 2019), and Transformers (Nie et al., 2022; Liu et al., 2023). More recently, Large Time-Series Models (LTSMs), such as Timer (Liu et al., 2024b), Moirai (Woo et al., 2024), TimesFM (Das et al., 2024), Chronos (Ansari et al., 2024), Moment (Goswami et al., 2024), and Toto (Cohen et al., 2024), have emerged, leveraging large-scale pretraining for zero-shot forecasting.

Most TSF methods minimize predictive error while overlooking downstream integration, where forecast errors have unequal importance. This mismatch, observed in challenges such as *Predict+Optimize for Renewable Energy Scheduling* (Bergmeir et al., 2022) and the *M5 Competition* (Makridakis et al., 2022), highlights the need for models aligned with task-specific objectives. Prior work includes integrating learned weights into optimization (Bertsimas and Kallus, 2020), predictive loss functions tailored to optimization (Elmachtoub and Grigas, 2022), and broader E2E learning paradigms (Qi et al., 2023).

However, existing approaches assume fixed task specifications and static regions of importance. In practice, domains such as wireless traffic prediction (Wu et al., 2021b; Ping et al., 2013) demand adaptation to shifting priorities, for example, optimizing base-station deactivation during low-traffic periods or power allocation under extremes. Since such thresholds are rarely known a priori, TSF frameworks must allow post-hoc adjustment of importance during inference (Figure 1).

[*]École Polytechnique, Palaiseau, France (Research Intern)
[†]Paris Research Center, Huawei Technologies, Boulogne-Billancourt, France
[‡]Lead researcher for this study. Corresponding author: tareq.si.salem@huawei.com

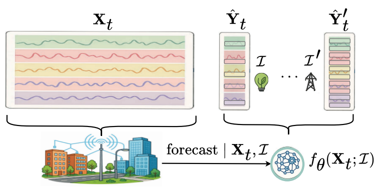

Figure 1: The figure depicts TSF in a wireless network, from data collection to training and downstream use. Applications include energy efficiency, which depends on forecasting low-traffic periods, and power allocation, requiring accuracy across traffic bands. Our method allows a single model to adapt to diverse tasks at inference, unlike traditional task-specific approaches.

**Contributions.** We address this gap by: (1) proposing a training methodology that enables multivariate TSF models to adapt to multiple downstream tasks at inference without retraining, (2) conducting extensive experiments on synthetic and real-world traces with comprehensive baselines and ablations, and (3) releasing a new wireless mobile network dataset to support future research.

## 2 The Forecasting Problem

**Time-Series.** A multivariate time-series is a temporally ordered sequence of vectors. Let $\mathbf{x}_t \in \mathbb{R}^n$ denote the $n$-dimensional observation at time $t \in [T]$, with $\mathbf{x}_t = (x_{t,i})_{i \in [n]}$. The series is $\{\mathbf{x}_1, \dots, \mathbf{x}_T\}$, where each component lies in a bounded set $\mathcal{X} \subset \mathbb{R}$. Temporal dependence is assumed, with $\mathbf{x}_t$ potentially influenced by past values $\mathbf{x}_{t-k}$ for $k > 0$.

**The Learning Problem.** TSF is cast as supervised regression by forming input-output pairs via sliding windows. For forecast horizon $\tau$ and window size $w$, the input is $\mathbf{X}_t = \mathbf{x}_{t-w:t-1} \in \mathcal{X}^{w \times n}$, and the target is $\mathbf{Y}_t = \mathbf{x}_{t:t+\tau-1} \in \mathcal{X}^{\tau \times n}$. We assume an underlying operator $f : \mathcal{X}^{w \times n} \to \mathcal{X}^{\tau \times n}$ with noisy observations $\mathbf{Y}_t = f(\mathbf{X}_t) + \boldsymbol{\epsilon}_t$. A parametric model $f_{\boldsymbol{\theta}}$ is trained on dataset $D = \{(\mathbf{X}_t, \mathbf{Y}_t)\}_{t=w}^{T-\tau}$ to minimize expected loss $\boldsymbol{\theta}_\star \in \arg\min_{\boldsymbol{\theta} \in \mathbb{R}^d} \mathbb{E}_{(\mathbf{X},\mathbf{Y}) \sim \mathcal{D}} \left[ l(f_{\boldsymbol{\theta}}(\mathbf{X}), \mathbf{Y}) \right]$. In practice, this is approximated by empirical risk with regularization $R(\boldsymbol{\theta})$ to control complexity and improve generalization (Shalev-Shwartz and Ben-David, 2014). Common choices of $l$ include Mean Squared Error (MSE), estimating conditional expectations, and Mean Absolute Error (MAE), estimating conditional medians.

## 3 Methodology

We investigate five training policies of increasing flexibility. We begin with a baseline policy (`B-Policy`) corresponding to standard TSF training that ignores interval specificity, followed by a task-specific policy (`E2E-Policy`) that optimizes for a single target interval, representing the E2E approach when downstream tasks are known. We then introduce a continuous-interval policy (`C-Policy`) that incorporates intervals as covariates, enabling inference-time flexibility by exposing the model to all possible intervals during training. However, as shown in our experiments, this approach suffers from instability and yields suboptimal results, motivating more structured alternatives. Next, we consider a discretized policy ($\mathtt{D}_L$`-Policy`) that samples from a fixed set of intervals covering the forecasting space, thereby reducing the interval search space. Since inference-time regions of interest need not align exactly with these discretized intervals, we propose a patching-augmented discretized policy ($\mathtt{D}^\star_L$`-Policy`), which combines finer discretization with a boundary-aware patching mechanism for improved adaptation.

**Baseline Policy** (`B-Policy`)**.** Follows the standard supervised training setup in Section 2, computing loss across the full forecasting domain $\mathcal{X}$, without interval awareness.

**Task-Specific Policy** (`E2E-Policy`)**.** Given a target interval $\mathcal{I} \subseteq \mathcal{X}$, this policy restricts the loss to $\mathcal{I}$. The model is learned by solving $\boldsymbol{\theta}_\star \in \arg\min_{\boldsymbol{\theta} \in \mathbb{R}^d} \mathbb{E}_{(\mathbf{X},\mathbf{Y}) \sim \mathcal{D}} [l(f_{\boldsymbol{\theta}}(\mathbf{X}), \mathbf{Y}) \cdot \mathbb{1}(\mathbf{Y} \in \mathcal{I}^{\tau \times n})]$.

**Continuous-Interval Policy** (`C-Policy`)**.** To generalize across intervals, we encode $\mathcal{I}$ as covariates (e.g., boundaries $[I_{\min}, I_{\max}] \in \mathcal{X}^2$). The model $f_{\boldsymbol{\theta}}$ thus maps $\mathcal{X}^{w \times n+2} \to \mathcal{X}^{\tau \times n}$. Intervals are sampled uniformly from $\mathcal{U}_\delta = \{\mathcal{I} \subseteq \mathcal{X} : |\mathcal{I}| \geq \delta\}$, where $\delta$ controls minimum length of an interval. The custom loss is $L(f_{\boldsymbol{\theta}}(\mathbf{X}_t, \mathcal{I}_t), \mathbf{Y}_t, \mathcal{I}_t) = l(f_{\boldsymbol{\theta}}(\mathbf{X}_t, \mathcal{I}_t), \mathbf{Y}_t) \cdot \mathbb{1}(\mathbf{Y}_t \in \mathcal{I}_t^{\tau \times n})$, and training minimizes the expectation over both $\mathcal{D}$ and $\mathcal{U}_\delta$. In this formulation, the model $\boldsymbol{\theta}$ explicitly conditions on both the input sequence $\mathbf{X}_t$ and the interval $\mathcal{I}_t$ to produce the forecast $\hat{\mathbf{Y}}_t = f_{\boldsymbol{\theta}}(\mathbf{X}_t, \mathcal{I}_t)$.

**Discretized-Interval Policy** (`D`$_L$`-Policy`). Instead of sampling from $\mathcal{U}_\delta$, intervals are drawn from a discrete set $\mathcal{C}_L$ of $L$ disjoint intervals covering $\mathcal{X}$, i.e., $\dot{\bigcup}_{\mathcal{I}\in\operatorname{supp}(\mathcal{C}_L)}\mathcal{I} = \mathcal{X}$.

**Patching-Augmented Policy** (`D`$_L^\star$`-Policy`). We refine `D`$_L$`-Policy` by introducing two key components: (1) a *patching mechanism* that integrates forecasts from constituent intervals to enhance predictions within a target interval of interest, and (2) a *soft boundary loss* (decay function) designed to mitigate uncertainty near patching boundaries. A decay function modulates boundary contributions $d_\nu(y,\mathcal{I}) = \exp\big(-\nu \max\big(0,\ |y-\Delta_{\text{avg}}| - \Delta_{\text{diff}}\big)\big)$, where $\Delta_{\text{avg}}$ and $\Delta_{\text{diff}}$ are the midpoint and half-length of $\mathcal{I}$.[4] As $\nu \to \infty$, this reduces to the indicator function. The weighted regression and classification losses are

$$L_\nu = l(f_{\boldsymbol\theta}(\mathbf{X}_t,\mathcal{I}_t),\mathbf{Y}_t)\prod_{i,t} d_\nu(y_{t,i},\mathcal{I}_t), \quad L'_\nu = l'(f^c_{\boldsymbol\theta}(\mathbf{X}_t,\mathcal{I}_t),\mathbb{1}(\mathbf{Y}_t\in\mathcal{I}_t))\prod_{i,t} d_\nu(y_{t,i},\mathcal{I}_t), \quad (1)$$

respectively. The joint training objective is then $\boldsymbol\theta_\star = \arg\min_{\boldsymbol\theta}\ \mathbb{E}_{(\mathbf{X},\mathbf{Y}),\mathcal{I}\sim\mathcal{C}_L}\big[L_\nu + \phi\cdot L'_\nu\big]$, where $\phi$ is a hyperparameter controlling the trade-off between regression and classification objectives.

At inference, given interval $\mathcal{I}$, we collect overlapping training intervals $\Xi_L(\mathcal{I}) \triangleq \{\mathcal{I}'\in\operatorname{supp}(\mathcal{C}_L) : \mathcal{I}'\cap\mathcal{I}\neq\emptyset\}$. Predictions are then combined by: (1) Averaging strategy (1-strategy): $\hat{\mathbf{Y}} = \sum_{\mathcal{I}'\in\Xi_L(\mathcal{I})} f^c_\theta(\mathbf{X},\mathcal{I}')f_\theta(\mathbf{X},\mathcal{I}')(\sum_{\mathcal{I}'\in\Xi_L(\mathcal{I})} f^c_\theta(\mathbf{X},\mathcal{I}'))^{-1}$, (2) Maximum confidence strategy ($\infty$-strategy): $\hat{\mathbf{Y}} = f_\theta(\mathbf{X}, \operatorname{argmax}_{\mathcal{I}'\in\Xi_L(\mathcal{I})} f^c_\theta(\mathbf{X},\mathcal{I}'))$.

## 4 Experiments

**Experimental Setup.** This section reports the numerical results obtained from the proposed training policies and evaluates their forecasting performance in comparison with multiple baseline methods. We begin by describing the forecasting models, training policies, benchmark datasets, and training configurations employed. This is followed by both qualitative and quantitative analyses of the various training strategies applied to these models.[5] We evaluate four state-of-the-art TSF models: iTransformer (Liu et al., 2024a), DLinear (Zeng et al., 2023), PatchTST (Nie et al., 2023), and TimeMixer (Wang et al., 2024); further details on how these architectures are augmented to incorporate interval covariates and a classification head are provided in the Experimental Appendix. We consider five training policies introduced in Section 3: `B-Policy`, `E2E-Policy`, `C-Policy`, `D`$_L$`-Policy`, and `D`$_L^\star$`-Policy`, where the symbol $\star$ specifies the patching method ($\star = 1$ for average patching and $\star = \infty$ for maximum-confidence patching). For benchmarking, we use both synthetic and real-world datasets: `SynthDS` (synthetic trace for controlled evaluation), `BLW-TrafficDS` (Fechete et al., 2025) (beam-level wireless traffic, released with this work), `Traffic` (Caltrans, 2016) (road occupancy), `Electricity` (Repository, 2014) (power consumption), and `Weather` (Wu et al., 2021a) (meteorological data). We provide additional results in the Experimental Appendix on the sensitivity of different policies to hyperparameters (e.g., number and length of sampled intervals, patching strategy, decay rate), as well as their impact on a realistic downstream energy-saving optimization task.

**Qualitative Comparison.** We begin with the `SynthDS` trace to illustrate how training policies adapt to intervals of interest. *Baseline:* Training with `B-Policy` yields averaged forecasts centered around the global mean (Fig. 4b), showing no adaptation to interval-specific distributions. *End-to-End:* Using `E2E-Policy` with $\mathcal{I} = [0.75, 1]$ (Fig. 2a) demonstrates best-case performance: forecasts align with the interval-specific signal but require retraining per interval. *Continuous Exploration:* Under `C-Policy`, the model must map all possible $\mathcal{I}\subset\mathcal{X}$ to their hypotheses. As shown in Fig. 2b, this approach underfits; restricting interval length ($|\mathcal{I}|\geq\delta$) improves results but introduces bias if $\delta$ is too large (Fig. 9). *Discrete Sampling:* With `D`$_L$`-Policy`, the model trains on a finite set of intervals (Fig. 2c). Performance matches `E2E-Policy` while retaining inference-time adaptability. However, it assumes prior knowledge of relevant intervals. *Patching:* To relax this assumption, we overparameterize the interval set and apply patching at inference (Figs. 2d, 2e). Despite slight degradation relative to `D`$_L$`-Policy`, patched models still recover the underlying hypotheses and adapt flexibly to unseen intervals, motivating their use in foundation TSF settings.

[4]This function is depicted in Figure 3.

[5]The code for all experiments is available at (Repository).

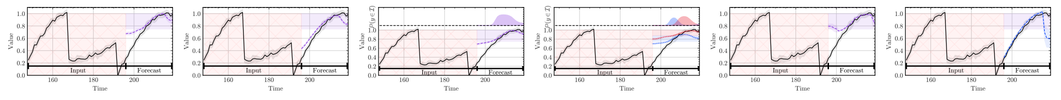

(a) (b) (c) (d) (e) (f)

Figure 2: Subfigures (a)–(f) present the performance of the iTransformer model trained on the `SynthDS` trace. Each subfigure corresponds to a different policy: `E2E`, `C`, $\mathtt{D}_4$, $\mathtt{D}_8$, $\mathtt{D}_8^1$, and `B`, respectively. The purple region marks the interval of interest, $\mathcal{I} = [0.75, 1.0]$. In the 1-strategy, eight intervals are patched into four. The filled region represents the classifier's predicted probability $\mathbb{P}(y \in \mathcal{I})$. Under the $\mathtt{D}_8^1$ policy, two intervals must be patched to generate a forecast for the selected interval $\mathcal{I}$. Black lines indicate target forecast values, while dashed lines denote the mean prediction over time, with shaded areas showing the standard deviation computed over 10 random seeds.

| Models | DLinear | | | | | | TimeMixer | | | | | | PatchTST | | | | | | iTransformer | | | | | |
|---|---|---|---|---|---|---|---|---|---|---|---|---|---|---|---|---|---|---|---|---|---|---|---|---|
| Policies / Intervals | $\mathtt{D}_L$ | $\mathtt{D}_{2L}^1$ | $\mathtt{D}_{2L}^\infty$ | B | $\mathtt{C}_{0.2}$ | **Improvement** | $\mathtt{D}_L$ | $\mathtt{D}_{2L}^1$ | $\mathtt{D}_{2L}^\infty$ | B | $\mathtt{C}_{0.2}$ | **Improvement** | $\mathtt{D}_L$ | $\mathtt{D}_{2L}^1$ | $\mathtt{D}_{2L}^\infty$ | B | $\mathtt{C}_{0.2}$ | **Improvement** | $\mathtt{D}_L$ | $\mathtt{D}_{2L}^1$ | $\mathtt{D}_{2L}^\infty$ | B | $\mathtt{C}_{0.2}$ | **Improvement** |
| **BLW-TrafficDS** ($\times\mathbf{10^3}$, $L=8$) | | | | | | | | | | | | | | | | | | | | | | | | |
| $\mathcal{I}_1$ | 167.1 | 172.3 | 164.9 | **163.8** | 218.0 | 0.0% | 127.5 | 148.1 | 138.0 | **125.9** | 143.7 | 0.0% | $\underline{\mathbf{102.8}}$ | 158.2 | 117.8 | 124.1 | 118.1 | 17.2% | **119.3** | 121.1 | 122.8 | 130.8 | 133.1 | 8.8% |
| $\mathcal{I}_2$ | 76.0 | **74.9** | 75.7 | 82.4 | 84.8 | 9.1% | 40.1 | **37.8** | 41.7 | 83.0 | 50.7 | 54.5% | 31.1 | $\underline{\mathbf{30.4}}$ | 35.3 | 77.9 | 34.6 | 60.9% | **74.7** | 75.9 | 75.7 | 77.3 | 75.6 | 3.4% |
| $\mathcal{I}_3$ | 56.7 | **56.0** | 56.7 | 62.0 | 58.8 | 9.7% | 24.3 | **22.9** | 23.8 | 64.9 | 32.0 | 64.7% | 18.3 | $\underline{\mathbf{17.2}}$ | 20.8 | 60.3 | 22.5 | 71.5% | 57.1 | 58.4 | 57.6 | 59.5 | **56.0** | 5.9% |
| $\mathcal{I}_4$ | 44.2 | 43.8 | 44.4 | 48.9 | **43.4** | 11.2% | 16.1 | **15.4** | 15.8 | 48.1 | 20.8 | 68.0% | 11.4 | $\underline{\mathbf{10.4}}$ | 12.6 | 47.2 | 15.2 | 78.0% | 44.0 | 44.6 | 44.1 | 46.8 | **42.1** | 10.0% |
| $\mathcal{I}_5$ | 33.5 | 33.4 | 33.8 | 37.6 | **31.7** | 15.7% | 10.8 | **10.2** | 10.4 | 35.8 | 13.1 | 71.5% | 7.1 | $\underline{\mathbf{6.5}}$ | 7.9 | 34.9 | 9.8 | 81.4% | 31.4 | 32.1 | 31.9 | 35.5 | **28.7** | 19.2% |
| $\mathcal{I}_6$ | 28.1 | 27.9 | 28.2 | 31.8 | **26.4** | 16.9% | 8.0 | **7.8** | 8.0 | 30.2 | 9.3 | 74.2% | 4.5 | $\underline{\mathbf{4.0}}$ | 5.0 | 29.4 | 6.8 | 86.3% | 25.2 | 25.7 | 25.7 | 29.8 | **23.3** | 21.8% |
| $\mathcal{I}_7$ | 19.3 | 19.2 | 19.4 | 21.7 | **18.8** | 13.4% | **5.5** | 5.5 | 5.6 | 21.8 | 6.1 | 74.8% | 2.7 | $\underline{\mathbf{2.4}}$ | 2.8 | 20.4 | 3.9 | 88.2% | 19.2 | 19.5 | 19.5 | 20.6 | **18.1** | 12.1% |
| $\mathcal{I}_8$ | 11.1 | 11.1 | 11.2 | 12.5 | **10.9** | 12.8% | **3.3** | 3.5 | 3.4 | 12.1 | 3.6 | 72.7% | 1.7 | $\underline{\mathbf{1.5}}$ | 1.8 | 11.7 | 2.6 | 87.2% | **11.2** | 11.2 | 11.2 | 11.8 | 11.4 | 5.1% |
| $\overline{\mathcal{I}_1\text{–}\mathcal{I}_8}$ | **54.0** | 54.8 | 54.3 | 57.6 | 61.6 | 6.3% | **29.4** | 31.4 | 30.9 | 52.7 | 34.9 | 44.2% | $\underline{\mathbf{22.4}}$ | 28.8 | 25.5 | 50.7 | 26.7 | 55.8% | **47.8** | 48.6 | 48.6 | 51.5 | 48.5 | 7.2% |
| `Traffic` ($\times$**500**, $L=4$) | | | | | | | | | | | | | | | | | | | | | | | | |
| $\mathcal{I}_1$ | 1.70 | **1.53** | 1.67 | 1.79 | 1.82 | 14.5% | 1.90 | **1.71** | 1.73 | 2.44 | 2.17 | 29.9% | $\underline{\mathbf{1.08}}$ | 1.02 | 1.06 | 1.41 | 1.11 | 27.7% | 1.29 | **1.30** | 1.32 | 1.41 | 1.36 | 8.5% |
| $\mathcal{I}_2$ | 1.65 | **1.35** | 1.44 | 1.99 | 1.71 | 32.2% | 1.25 | **1.23** | 1.27 | 2.02 | 1.52 | 39.2% | 0.91 | 0.90 | 0.93 | 1.42 | $\underline{\mathbf{0.89}}$ | 37.3% | **1.19** | 1.22 | 1.24 | 1.50 | 1.13 | 20.7% |
| $\mathcal{I}_3$ | 0.61 | **0.44** | 0.47 | 0.81 | 0.62 | 45.7% | 0.39 | **0.36** | 0.41 | 0.74 | 0.51 | 51.5% | $\underline{\mathbf{0.32}}$ | 0.30 | 0.35 | 0.65 | 0.30 | 53.9% | 0.53 | **0.54** | 0.55 | 0.66 | 0.53 | 19.7% |
| $\mathcal{I}_4$ | 0.45 | **0.31** | 0.33 | 0.59 | 0.45 | 47.5% | 0.22 | **0.20** | 0.24 | 0.59 | 0.35 | 66.2% | 0.16 | $\underline{\mathbf{0.16}}$ | 0.19 | 0.53 | 0.16 | 69.8% | 0.35 | **0.36** | 0.37 | 0.51 | 0.35 | 31.4% |
| $\overline{\mathcal{I}_1\text{–}\mathcal{I}_4}$ | 1.10 | **0.90** | 0.98 | 1.29 | 1.15 | 30.2% | 0.94 | **0.88** | 0.91 | 1.45 | 1.14 | 39.3% | 0.62 | $\underline{\mathbf{0.59}}$ | 0.63 | 1.01 | 0.62 | 41.6% | **0.84** | 0.85 | 0.87 | 1.02 | 0.84 | 17.6% |
| `Weather` ($\times$**2**, L = 4) | | | | | | | | | | | | | | | | | | | | | | | | |
| $\mathcal{I}_1$ | 1.05 | 0.76 | **0.75** | 0.78 | 1.32 | 3.9% | 2.25 | **0.73** | 0.71 | 1.00 | 1.94 | 27.0% | $\underline{\mathbf{0.40}}$ | 0.67 | 0.53 | 0.65 | 1.17 | 38.5% | 0.49 | **0.48** | 0.49 | 0.68 | 1.72 | 29.4% |
| $\mathcal{I}_2$ | 0.36 | **0.23** | 0.29 | 0.42 | 0.36 | 45.2% | 0.37 | **0.22** | 0.26 | 0.54 | 0.43 | 59.3% | $\underline{\mathbf{0.22}}$ | 0.23 | 0.28 | 0.37 | 0.22 | 40.5% | **0.32** | 0.32 | 0.32 | 0.42 | 0.49 | 23.8% |
| $\mathcal{I}_3$ | 0.13 | **0.09** | 0.10 | 0.20 | 0.26 | 55.0% | 0.19 | **0.08** | 0.09 | 0.26 | 0.25 | 69.2% | $\underline{\mathbf{0.08}}$ | 0.09 | 0.11 | 0.22 | 0.08 | 63.6% | 0.18 | **0.17** | 0.18 | 0.23 | 0.39 | 26.1% |
| $\mathcal{I}_4$ | 0.16 | **0.14** | 0.21 | 0.21 | 0.27 | 33.3% | 0.17 | **0.12** | 0.13 | 0.27 | 0.26 | 55.6% | $\underline{\mathbf{0.10}}$ | 0.13 | 0.14 | 0.23 | 0.11 | 56.5% | 0.19 | **0.19** | 0.19 | 0.21 | 0.38 | 9.5% |
| $\overline{\mathcal{I}_1\text{–}\mathcal{I}_4}$ | 0.43 | **0.31** | 0.34 | 0.40 | 0.55 | 22.5% | 0.75 | **0.29** | 0.30 | 0.52 | 0.72 | 44.2% | $\underline{\mathbf{0.20}}$ | 0.28 | 0.26 | 0.37 | 0.40 | 46.0% | **0.30** | 0.29 | 0.29 | 0.38 | 0.74 | 23.7% |
| `Electricity` ($\times\mathbf{10^{-1}}$, $L=4$) | | | | | | | | | | | | | | | | | | | | | | | | |
| $\mathcal{I}_1$ | 3.81 | 3.82 | 3.82 | **3.77** | 3.95 | 0.0% | **3.83** | 3.95 | 3.95 | 4.50 | 4.86 | 14.9% | 3.33 | 4.66 | 4.69 | $\underline{\mathbf{3.32}}$ | 3.78 | 0.0% | 12.8 | 10.3 | 10.5 | **3.26** | 3.67 | 0.0% |
| $\mathcal{I}_2$ | 1.15 | 1.16 | 1.16 | 1.17 | **1.14** | 2.23% | 1.11 | **1.07** | 1.09 | 1.41 | 1.37 | 24.3% | $\underline{\mathbf{0.919}}$ | 1.24 | 1.34 | 1.01 | 0.990 | 9.37% | **4.67** | 3.69 | 3.84 | 1.05 | 1.02 | 2.48% |
| $\mathcal{I}_3$ | 0.916 | 0.929 | 0.932 | 0.955 | **0.890** | 6.81% | 0.807 | **0.782** | 0.836 | 1.08 | 0.984 | 27.6% | $\underline{\mathbf{0.671}}$ | 0.852 | 0.931 | 0.835 | 0.689 | 19.6% | 2.08 | 1.84 | 1.98 | 0.861 | **0.822** | 4.53% |
| $\mathcal{I}_4$ | 0.369 | 0.379 | 0.380 | 0.399 | **0.353** | 7.52% | 0.297 | **0.277** | 0.288 | 0.449 | 0.388 | 38.3% | $\underline{\mathbf{0.238}}$ | 0.248 | 0.272 | 0.370 | 0.243 | 35.7% | 0.567 | **0.509** | 0.522 | 0.372 | 0.322 | 13.4% |
| $\overline{\mathcal{I}_1\text{–}\mathcal{I}_4}$ | **1.56** | 1.57 | 1.57 | 1.57 | 1.58 | 0.7% | **1.51** | 1.52 | 1.54 | 1.86 | 1.90 | 18.8% | $\underline{\mathbf{1.29}}$ | 1.75 | 1.81 | 1.39 | 1.42 | 6.93% | 5.02 | 4.09 | 4.21 | **1.39** | 1.46 | 0.0% |
| `SynthDS` ($\times\mathbf{10^3}$, $L=4$) | | | | | | | | | | | | | | | | | | | | | | | | |
| $\mathcal{I}_1$ | 15.0 | **14.5** | 18.5 | 50.9 | 24.8 | 71.5% | 16.2 | **15.7** | 17.9 | 45.5 | 17.5 | 65.5% | $\underline{\mathbf{13.2}}$ | 13.2 | 15.1 | 37.9 | 15.3 | 65.2% | 14.1 | **14.1** | 17.5 | 40.2 | 20.0 | 65.0% |
| $\mathcal{I}_2$ | **11.7** | 11.9 | 12.8 | 20.3 | 12.8 | 42.4% | **11.4** | 12.2 | 15.0 | 18.8 | 13.5 | 39.4% | **9.08** | 10.2 | 11.2 | 26.8 | 11.0 | 66.2% | $\underline{\mathbf{7.96}}$ | 9.17 | 9.65 | 26.2 | 10.6 | 69.6% |
| $\mathcal{I}_3$ | 11.7 | 11.2 | 10.7 | 17.1 | **10.6** | 38.1% | 11.5 | 11.7 | 13.3 | 13.9 | **10.8** | 22.4% | $\underline{\mathbf{7.74}}$ | 8.61 | 8.92 | 14.9 | 9.19 | 48.0% | **7.97** | 8.38 | 8.63 | 16.2 | 8.71 | 50.9% |
| $\mathcal{I}_4$ | 16.8 | **16.8** | 18.2 | 41.0 | 20.3 | 59.1% | **15.5** | 17.3 | 19.7 | 34.9 | 16.6 | 55.5% | **12.7** | 12.9 | 13.3 | 36.8 | 13.7 | 65.6% | 13.1 | **12.4** | 13.6 | 33.7 | 13.4 | 63.2% |
| $\overline{\mathcal{I}_1\text{–}\mathcal{I}_4}$ | 13.8 | **13.6** | 15.1 | 32.3 | 17.1 | 57.9% | **13.7** | 14.2 | 16.5 | 28.3 | 14.6 | 51.7% | $\underline{\mathbf{10.7}}$ | 11.2 | 12.1 | 29.1 | 12.3 | 63.3% | **10.8** | 11.0 | 12.3 | 29.1 | 13.2 | 62.9% |

Table 1: MAE (↓) and relative improvement (↑) over the baseline for `DLinear`, `TimeMixer`, `iTransformer`, and `PatchTST` under five policies. MAE values are rescaled per dataset ($\times 10^3$ for `SynthDS/BLW-TrafficDS`, $\times 500$ for `Traffic`, $\times 2$ for `Weather`, $\times 10^{-1}$ for `Electricity`). For `BLW-TrafficDS`, patching uses $L = 8, 16$ intervals. Bold indicates best per model; underline marks overall best.

**Quantitative Comparison.** Table 1 reports MAE across datasets and models. As expected, `B-Policy` performs worst, while `C-Policy` yields modest gains but struggles to separate hypotheses. $\mathtt{D}_L$`-Policy` improves markedly when its intervals match ground truth, though this assumption is unrealistic in practice. $\mathtt{D}_L^\star$`-Policy` maintains comparable accuracy while enabling broader adaptability, and in some cases even surpasses the discrete baseline due to ensemble-like effects. These trends extend to real-world datasets, with stronger models (iTransformer, PatchTST) benefiting most, while weaker ones (DLinear) show less consistent improvements. Overall, patching provides a practical compromise between performance and flexibility.

## 5 Conclusion

This work introduces a training methodology that extends existing TSF models into foundation-style architectures capable of inference-time adaptation to diverse downstream tasks. Extensive empirical evaluation confirms the effectiveness of the proposed approach. Future directions include scaling to broader domains and adapting large pre-trained TSF models (Liu et al., 2024b; Woo et al., 2024; Das et al., 2024; Ansari et al., 2024; Goswami et al., 2024; Cohen et al., 2024) for arbitrary-interval forecasting.

## References

3GPP (2014). Evolved universal terrestrial radio access (e-utra); potential solutions for energy saving for e-utran (study on energy saving enhancement for e-utran). Technical Report TR 36.927 (v12.0.0, Release 12), 3GPP / ETSI.

Ansari, A. F., Stella, L., Turkmen, C., Zhang, X., Mercado, P., Shen, H., Shchur, O., Rangapuram, S., Arango, S. P., Kapoor, S., et al. (2024). Chronos: Learning the language of time series.

Bergmeir, C., de Nijs, F., Sriramulu, A., Abolghasemi, M., Bean, R., Betts, J., Bui, Q., Dinh, N. T., Einecke, N., Esmaeilbeigi, R., et al. (2022). Comparison and evaluation of methods for a predict+ optimize problem in renewable energy. *arXiv preprint arXiv:2212.10723*.

Bertsimas, D. and Kallus, N. (2020). From predictive to prescriptive analytics. *Management Science*, 66(3):1025–1044.

Brown, R. G. (1956). *Exponential smoothing for predicting demand*. Little.

Caltrans (2016). Pems traffic data. `http://pems.dot.ca.gov`.

Celebi, H., Yapıcı, Y., Güvenç, I., and Schulzrinne, H. (2019). Load-based on/off scheduling for energy-efficient delay-tolerant 5g networks. *IEEE Transactions on Green Communications and Networking*, 3(4):955–970.

Chen, C., Petty, K., Skabardonis, A., Varaiya, P., and Jia, Z. (2001). Freeway performance measurement system: mining loop detector data. *Transportation research record*, 1748(1):96–102.

Cohen, B., Khwaja, E., Wang, K., Masson, C., Ramé, E., Doubli, Y., and Abou-Amal, O. (2024). Toto: Time series optimized transformer for observability. *arXiv preprint arXiv:2407.07874*.

Das, A., Kong, W., Sen, R., and Zhou, Y. (2024). A decoder-only foundation model for time-series forecasting. In *Forty-first International Conference on Machine Learning*.

Elmachtoub, A. N. and Grigas, P. (2022). Smart "predict, then optimize". *Management Science*, 68(1):9–26.

Fechete, L. et al. (2025). Goal-oriented time-series forecasting: Foundation framework design. Dataset: Beam-Level (5G) Time-Series Dataset, `https://huggingface.co/datasets/netop/Beam-Level-Traffic-Timeseries-Dataset`.

Ghassemi, M., Pimentel, M., Naumann, T., Brennan, T., Clifton, D., Szolovits, P., and Feng, M. (2015). A multivariate timeseries modeling approach to severity of illness assessment and forecasting in icu with sparse, heterogeneous clinical data. In *Proceedings of the AAAI conference on artificial intelligence*, volume 29.

Goswami, M., Szafer, K., Choudhry, A., Cai, Y., Li, S., and Dubrawski, A. (2024). Moment: A family of open time-series foundation models. *arXiv preprint arXiv:2402.03885*.

Granger, C. W. J. and Newbold, P. (2014). *Forecasting economic time series*. Academic press.

He, Y. and Zhao, J. (2019). Temporal convolutional networks for anomaly detection in time series. In *Journal of Physics: Conference Series*, volume 1213, page 042050. IOP Publishing.

Hyndman, R. J. and Athanasopoulos, G. (2015). 8.9 seasonal arima models. *Forecasting: principles and practice. oTexts. Retrieved*, 19.

Ju, H., Kim, S., Kim, Y., and Shim, B. (2022). Energy-efficient ultra-dense network with deep reinforcement learning. *IEEE Transactions on Wireless Communications*, 21(8):6539–6552.

Li, N., Arnold, D. M., Down, D. G., Barty, R., Blake, J., Chiang, F., Courtney, T., Waito, M., Trifunov, R., and Heddle, N. M. (2022). From demand forecasting to inventory ordering decisions for red blood cells through integrating machine learning, statistical modeling, and inventory optimization. *Transfusion*, 62(1):87–99.

Liu, Y., Hu, T., Zhang, H., Wu, H., Wang, S., Ma, L., and Long, M. (2023). itransformer: Inverted transformers are effective for time series forecasting. *arXiv preprint arXiv:2310.06625*.

Liu, Y., Hu, T., Zhang, H., Wu, H., Wang, S., Ma, L., and Long, M. (2024a). itransformer: Inverted transformers are effective for time series forecasting.

Liu, Y., Zhang, H., Li, C., Huang, X., Wang, J., and Long, M. (2024b). Timer: Transformers for time series analysis at scale. *arXiv e-prints*, pages arXiv–2402.

Loshchilov, I. and Hutter, F. (2017). Decoupled weight decay regularization. *arXiv preprint arXiv:1711.05101*.

Lozano, J. X. S., Ayala-Romero, J. A., Garcia-Saavedra, A., and Costa-Perez, X. (2025). Kairos: Energy-efficient radio unit control for o-ran via advanced sleep modes. In *IEEE INFOCOM 2025-IEEE Conference on Computer Communications*, pages 1–10. IEEE.

Makridakis, S., Spiliotis, E., and Assimakopoulos, V. (2022). M5 accuracy competition: Results, findings, and conclusions. *International Journal of Forecasting*, 38(4):1346–1364.

Martín, L., Zarzalejo, L. F., Polo, J., Navarro, A., Marchante, R., and Cony, M. (2010). Prediction of global solar irradiance based on time series analysis: Application to solar thermal power plants energy production planning. *Solar Energy*, 84(10):1772–1781.

Nie, Y., Nguyen, N. H., Sinthong, P., and Kalagnanam, J. (2022). A time series is worth 64 words: Long-term forecasting with transformers. *arXiv preprint arXiv:2211.14730*.

Nie, Y., Nguyen, N. H., Sinthong, P., and Kalagnanam, J. (2023). A time series is worth 64 words: Long-term forecasting with transformers.

Ping, S., Aijaz, A., Holland, O., and Aghvami, A. H. (2013). Green cellular access network operation through dynamic spectrum and traffic load management. In *2013 IEEE 24th Annual International Symposium on Personal, Indoor, and Mobile Radio Communications (PIMRC)*, pages 2791–2796.

Qi, M., Shi, Y., Qi, Y., Ma, C., Yuan, R., Wu, D., and Shen, Z.-J. (2023). A practical end-to-end inventory management model with deep learning. *Management Science*, 69(2):759–773.

Qian, Z., Pei, Y., Zareipour, H., and Chen, N. (2019). A review and discussion of decomposition-based hybrid models for wind energy forecasting applications. *Applied energy*, 235:939–953.

Ray, E. L., Wang, Y., Wolfinger, R. D., and Reich, N. G. (2025). Flusion: Integrating multiple data sources for accurate influenza predictions. *Epidemics*, 50:100810.

Repository, U. M. L. (2014). Electricityloaddiagrams20112014. `https://archive.ics.uci.edu/ml/datasets/ElectricityLoadDiagrams20112014`.

Shalev-Shwartz, S. and Ben-David, S. (2014). *Understanding machine learning: From theory to algorithms*. Cambridge university press.

Siami-Namini, S., Tavakoli, N., and Namin, A. S. (2019). The performance of lstm and bilstm in forecasting time series. In *2019 IEEE International conference on big data (Big Data)*, pages 3285–3292. IEEE.

Wang, S., Wu, H., Shi, X., Hu, T., Luo, H., Ma, L., Zhang, J. Y., and Zhou, J. (2024). Timemixer: Decomposable multiscale mixing for time series forecasting.

Woo, G., Liu, C., Kumar, A., Xiong, C., Savarese, S., and Sahoo, D. (2024). Unified training of universal time series forecasting transformers.

Wu, H., Xu, J., Wang, J., and Long, M. (2021a). Autoformer: Decomposition transformers with auto-correlation for long-term series forecasting. *Advances in neural information processing systems*, 34:22419–22430.

Wu, H., Zhou, H., Long, M., and Wang, J. (2023). Interpretable weather forecasting for worldwide stations with a unified deep model. *Nature Machine Intelligence*, 5(6):602–611.

Wu, Q., Chen, X., Zhou, Z., Chen, L., and Zhang, J. (2021b). Deep reinforcement learning with spatio-temporal traffic forecasting for data-driven base station sleep control. *IEEE/ACM transactions on networking*, 29(2):935–948.

Zeng, A., Chen, M., Zhang, L., and Xu, Q. (2023). Are transformers effective for time series forecasting? In *Proceedings of the AAAI conference on artificial intelligence*, volume 37, pages 11121–11128.

Zhang, J. and Man, K.-F. (1998). Time series prediction using rnn in multi-dimension embedding phase space. In *SMC'98 conference proceedings. 1998 IEEE international conference on systems, man, and cybernetics (cat. no. 98CH36218)*, volume 2, pages 1868–1873. IEEE.

## A Detailed Experimental Setup

**Time-Series Forecasting Models.** We evaluate four state-of-the-art TSF models: iTransformer (Liu et al., 2024a), DLinear (Zeng et al., 2023), PatchTST (Nie et al., 2023), and TimeMixer (Wang et al., 2024). To incorporate target interval information $\mathcal{I}$, we modify each architecture accordingly. Given an interval of interest $\mathcal{I} \subseteq \mathcal{X}$, the vectorized form of $\mathcal{I}$ is concatenated with the temporal encoding in iTransformer, while for DLinear, PatchTST, and TimeMixer, it is introduced as two additional temporal channels. We further extend these regression models to support a dual-task objective—forecasting and classification—by adding a classification head. This is implemented by doubling the output dimension of the final projection layer (equal to the forecasting horizon $\tau$) and partitioning it into regression outputs (first $\tau$ dimensions) and classification logits (remaining $\tau$ dimensions). This enables the models to both predict future values and estimate the probability that these forecasts fall within the target interval $\mathcal{I}$.

**Benchmarking Datasets.** In our experimental evaluation, we employ several benchmark datasets to substantiate our claims:

1. `SynthDS` is a synthetic dataset designed to highlight the various components of our proposed methodology. The trace is constructed by combining an input signal

$$\left(\sin\left(\frac{\pi n}{2D}\right)\right)_{n\in[w]}, \tag{2}$$

   where $w = 24$ denotes the signal length, with an output signal selected uniformly at random (u.a.r.) from the set

$$\left\{\frac{1}{4}\left(\sin\left(\frac{\pi}{2w}n + \frac{\pi}{2}\right) + k\right)_{n\in[w]} : k \in [4]\right\}. \tag{3}$$

   To produce a trace spanning $T = 3.1 \times 10^3$ timesteps, the same randomly selected signal is concatenated multiple times. Gaussian noise with mean and standard deviation $0.05$ is then added to the trace. A noise-free version, without the addition of Gaussian noise, is shown in Figure 4a.
2. `BLW-TrafficDS` (Fechete et al., 2025) is released to the public domain as part of this study. We consider a subset of the DLPRB modality, which contains wireless beam-level measurements for $100$ beams over $10^3$ timesteps.
3. `Traffic` (Caltrans, 2016) contains hourly road occupancy rates (ranging from 0 to 1) collected by sensors on San Francisco Bay Area freeways between 2015 and 2016, covering a total of 48 months.
4. `Electricity` (Repository, 2014) records hourly electricity consumption (in kWh) for 321 clients from 2012 to 2014.
5. `Weather` (Wu et al., 2021a) contains 21 meteorological variables, including air temperature and humidity, recorded every 10 minutes throughout 2020.

**Training Configuration.** To ensure the reproducibility of our experiments, we provide a comprehensive description of the training setup. The datasets were divided into training, validation, and testing subsets. A 66-17-17 split was used for the `SynthDS`, `Traffic`, `Electricity`, and `Weather` datasets, while the `BLW-TrafficDS` dataset used a 70-10-20 split. Four state-of-the-art time series forecasting models—iTransformer, DLinear, PatchTST, and TimeMixer—were evaluated across the designated tasks.

The `BLW-TrafficDS`, `Traffic`, `Electricity`, and `Weather` datasets were processed using a multivariate-to-multivariate configuration, whereas the `SynthDS` dataset used a univariate-to-univariate setup. Input sequence lengths and forecasting horizons were tailored to each dataset: 48/24 for `SynthDS`, 96/24 for `BLW-TrafficDS`, and 168/48 for `Traffic`, `Electricity`, and `Weather`. The number of input channels was cropped to 100 for all datasets except `Weather`, which used 21 channels due to its limited dimensionality.

Model configurations across all experiments included 3 layers with a model dimension of 256. TimeMixer was configured with a channel dimension of 100. All models were trained with a batch size of 32 for 50 epochs. The AdamW optimizer (Loshchilov and Hutter, 2017) was used with

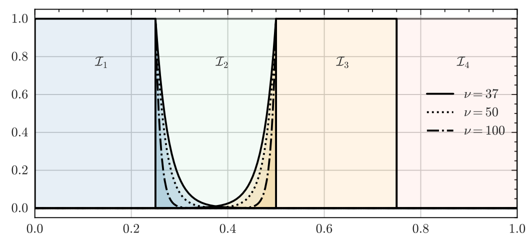

Figure 3: Impact of decay on the overlap of four intervals spanning the range $[0, 1]$. The figure illustrates the weighting associated with the intervals $\mathcal{I}_1 = [0, 0.25]$ and $\mathcal{I}_3$ for various decay rates $\nu \in \{37, 50, 100\}$. Note how increasing the decay rate reduces the overlap between the intervals. For $\nu = 37$, the weight value reaches $1\%$ at the midpoint of the adjacent interval.

an initial learning rate of $10^{-3}$ and a cosine annealing schedule with $\eta\_\min = 10^{-5}$, defined as:$\eta_t = \eta_{\min} + 0.5(\eta_{\max} - \eta_{\min})(1 + \cos(\pi \cdot t/n_{\text{epochs}}))$.

The MAE loss was used for regression tasks, while Binary Cross Entropy loss was applied for classification tasks when applicable. Early stopping with a patience of 5 epochs and checkpoint saving mechanisms were employed to reduce overfitting. Validation loss was computed as the average loss over each training interval.

The $\mathtt{D}_L^\star$`-Policy` was evaluated using 4 and 8 intervals for the `SynthDS`, `Traffic`, `Electricity`, and `Weather` datasets, and 8 and 16 intervals for the `BLW-TrafficDS` dataset. Interval endpoint sampling was performed per sample within each batch and incorporated into the forward pass as detailed in Section 3.

The dataset sizes are as follows: `SynthDS`—3,456 points, `BLW-TrafficDS`—1,025 points, `Weather`—52,696 points, `Traffic`—17,544 points, and `Electricity`—26,304 points. To set forecasting boundaries, the maximum values were assigned as $\max(\mathcal{X}) \in \{0.2, 500.0, 10000.0\}$ for `Traffic`, `Weather`, and `Electricity`, respectively. All experiments were executed on a system with 6 Tesla V100/16GB GPUs and an Intel(R) Xeon(R) Platinum 8164 CPU (104 cores).

## B Implications for Downstream Task: Forecasting for Energy-Saving

We consider a heterogeneous wireless network comprising two tiers: a *capacity cell* (e.g., a small or micro cell) providing high-throughput service within a localized area, and an overlaid *coverage cell* (e.g., a macro cell) ensuring broad-area connectivity. Two-tier architectures with dynamic small cell control have emerged as a key strategy for balancing spectral efficiency and energy savings in 5G and beyond (Celebi et al., 2019; Ju et al., 2022; Wu et al., 2021b; Lozano et al., 2025; 3GPP, 2014). In particular, recent work has shown that monitoring DLPRB utilization provides an effective signal for real-time sleep mode activation in energy-aware networks. We assume that the capacity cell can be selectively deactivated to reduce energy consumption when traffic demand is low. To govern this behavior, we adopt a threshold-based energy-saving policy that operates based on the observed DLPRB utilization. This mirrors widely-used control strategies that compare traffic load against fixed or learned thresholds to trigger cell activation or sleep (Celebi et al., 2019; Ju et al., 2022).

Let $u(t) \in [0, 1]$ denote the normalized DLPRB utilization at discrete time index $t \in \mathbb{Z}_{\geq 0}$, and let $u_{\text{th}} \in [0, 1]$ represent a fixed utilization threshold. The binary state variable $S(t) \in \{0, 1\}$ indicates whether the capacity cell is active ($S(t) = 1$) or deactivated ($S(t) = 0$). The policy is defined as:

$$S(t) = \begin{cases} 1, & \text{if } u(t) \geq u_{\text{th}}, \\ 0, & \text{otherwise.} \end{cases} \tag{4}$$

The instantaneous cell traffic load, denoted $L(t)$, is computed as the product of DLPRB utilization and the maximum throughput capacity of the capacity cell:

$$L(t) \triangleq u(t) \cdot C_{\text{cap}}, \tag{5}$$

where $C_{\text{cap}} > 0$ is the peak service rate (in Mbps) of the capacity cell.

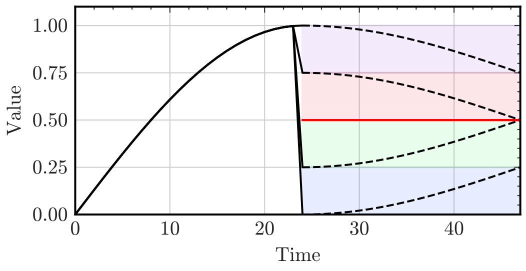

(a) Noise-free hypotheses in `SynthDS`

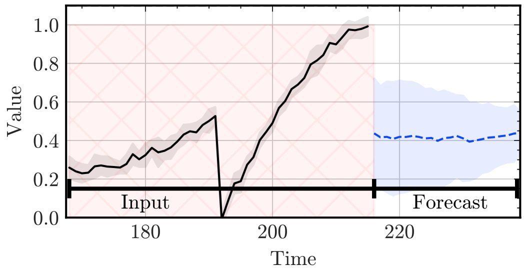

(b) Averaging tendencies of `B-Policy`

Figure 4: Subfigure (a) depicts the expected hypotheses used to construct the synthetic trace `SynthDS`. Subfigure (b) depicts the inability of the baseline policy `B-Policy` to distinguish between the different patterns in `SynthDS` dataset, as it predicts the average hypothesis (red line at 0.5). The model used is a trained iTransformer. Each subplot shows a time-shift of six steps. The black dotted line indicates the true values. The blue line shows the model's predictions. over 10 random seeds.

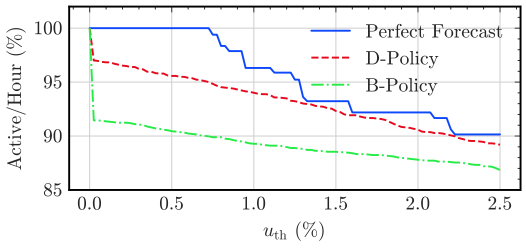

Figure 5: The impact of forecasting accuracy on wireless network energy saving as downstream application.

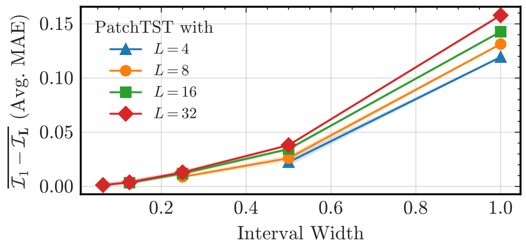

Figure 6: Comparison of the performance of the $\text{D}_4, \text{D}_8, \text{D}_{16}$ and $\text{D}_{32}$ policies with a fixed decay rate for the PatchTST model. The MAE is averaged across the different intervals.

**Realized Throughput.** The realized throughput, $R(t)$, is constrained by the physical limits of the serving infrastructure. When the capacity cell is active, it serves the traffic directly, up to its maximum capacity. If deactivated, the traffic is offloaded to the coverage cell, subject to its own

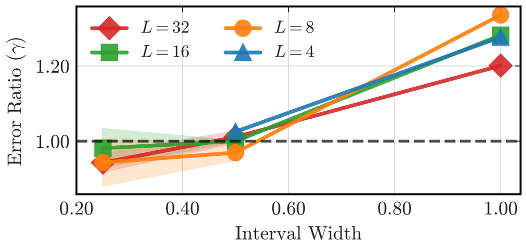

Figure 7: Comparison of the error ratio $\gamma$ across discretizations. Values $\gamma < 1$ indicate that the $\infty$-strategy performs better, while $\gamma > 1$ favors the 1-strategy.

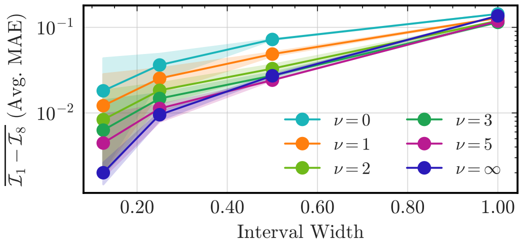

Figure 8: Comparison of the performance of the different decay rates for the PatchTST model trained with the $\mathtt{D}_8$-Policy.

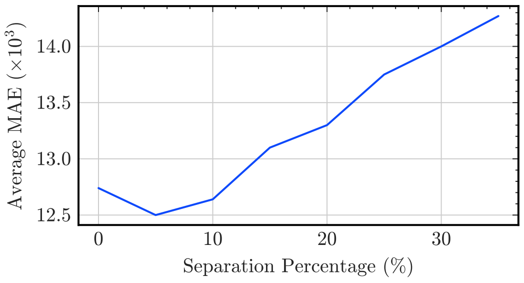

Figure 9: Interval-separation percentage ($\delta$) impact on `C-Policy`.

capacity constraint and a possible degradation in service quality. This is formalized as:

$$R(t) = \begin{cases} \min\left(L(t), C_{\text{cap}}\right), & \text{if } S(t) = 1, \\ \alpha \cdot \min\left(L(t), C_{\text{cov}}\right), & \text{if } S(t) = 0, \end{cases} \tag{6}$$

where $C_{\text{cov}} > 0$ denotes the capacity of the coverage cell and $\alpha \in (0, 1]$ is a degradation factor that accounts for reduced performance when traffic is offloaded.

**Energy Consumption.** To evaluate the energy-performance trade-off, we associate an energy cost with each state. Let $E_{\text{on}}$ and $E_{\text{off}}$ represent the per-time-unit energy consumption when the capacity cell is active or inactive, respectively. The total energy consumption at time $t$ is then:

$$E(t) = S(t) \cdot E_{\text{on}} + (1 - S(t)) \cdot E_{\text{off}}. \tag{7}$$

Over a time horizon of $T$ intervals, the average throughput and average energy consumption are given by:

$$\bar{R} = \frac{1}{T} \sum_{t=1}^{T} R(t), \quad \bar{E} = \frac{1}{T} \sum_{t=1}^{T} E(t). \tag{8}$$

This model captures the core dynamics of a load-aware energy-saving policy in a two-tier network, balancing energy efficiency with service quality under realistic physical constraints.

**Downstream Application Optimization Problem.** We consider the following optimization problem that balances average throughput and energy consumption:

$$\max_{u_{\mathrm{th}} \in [0,1]} \quad (1-\lambda)\,\bar{R}(u_{\mathrm{th}}) - \lambda\,\bar{E}(u_{\mathrm{th}}) \tag{9}$$

where $\lambda \in [0, 1]$ is a scalar trade-off parameter that governs the relative importance of energy efficiency versus throughput performance. Let $u^{\star}_{\mathrm{th}}(\lambda)$ denote the optimal threshold that solves problem (9) for a given value of $\lambda$.

**Instantiation and Numerical Results.** We instantiate the problem using representative parameter values from prior work (Celebi et al., 2019; Ju et al., 2022). In particular, the capacity cell peak throughput was set to $C_{\mathrm{cap}} = 100$ Mbps, while the coverage cell peak throughput was $C_{\mathrm{cov}} = 30$ Mbps. An offloading degradation factor of $\alpha = 0.5$ was applied to model performance reduction during traffic redirection. The energy consumption of a capacity cell was configured as $E_{\mathrm{on}} = 1266$ Wh when active and $E_{\mathrm{off}} = 320$ Wh when inactive. These parameters define the operational conditions under which forecasting models were evaluated.

Specifically, we train the iTransformer model on the `BLW-TrafficDS` dataset under two distinct policies: the `B-Policy` and the $\mathtt{D}^{\star}_{L}$`-Policy` ($L = 4$ intervals), with a forecasting horizon length of $H = 24$, with a test set rolled over 96 hours. We then evaluate and compare the performance of these policies. Since the threshold of interest is not known *a priori*, we deliberately select a slightly broader interval, $[0, 0.5]$, to ensure coverage; this involves patching together two intervals for the $\mathtt{D}^{\star}_{L}$`-Policy`. Based on the generated forecasts, we fix a threshold value and observe the resulting sequence of decisions, denoted as $S(t)$ for $t \in [T]$, where $T$ is the length of the forecast horizon. We analyze the discrepancies in sleep durations induced by the forecasts under the different policies and restrict our attention to a specific range of thresholds: $U_{\mathrm{th}} \in [0, 0.025]$.

As shown in Figure 5, the task-specific policy corresponding to a selected threshold yields decisions that are more closely aligned with the optimal policy—that is, the policy a decision-maker would follow with perfect foresight of future DLPRB values. This alignment demonstrates that the task-specific forecasts lead to better downstream optimization performance. Quantitatively, the task-specific policy produces forecasts that reduce the sleep duration error by a factor of three ($\times 3$), corresponding to an average reduction of one hour in sleep duration error per day. This improvement translates into an energy saving error of only 337 watts, in contrast to a significantly higher mismatch of $0.950$ kilowatts observed under the baseline policy per day.

## C Hyperparameter Sensitivity Analysis

We conducted experiments on the specific hyperparameters introduced by our work, namely the number of intervals $L$ in which we divided the time series domain $\mathcal{X}$, the decay rate $\nu \in [0, \infty]$ and the patching strategies (1-strategy and $\infty$-strategy).

**Interval Granularity ($L$).** Among the hyperparameters introduced, the number of intervals $L$ plays the most critical role. It determines the granularity of the discretization over the time series domain $\mathcal{X}$, directly influencing both model complexity and performance. Figure 6 illustrates the effect of varying $L$ on model performance. To assess this, we trained the PatchTST model on the `SynthDS`, under four instances of $\mathtt{D}^{\star}_{L}$`-Policy`. Each policy corresponds to a partitioning of the domain $\mathcal{X}$ into $L \in \{4, 8, 16, 32\}$ intervals, with a fixed decay rate $\nu$ across all runs. For evaluation, we measured the MAE over coarser partitions obtained via powers-of-two binning. The results demonstrate a clear trade-off: increasing the number of intervals improves granularity but may lead to decreased accuracy at coarser levels due to over-patching. This underscores the importance of selecting an appropriate value of $L$ to balance detail sensitivity with robustness across scales. For practical applications, a preliminary sweep over $L$ is recommended to identify the configuration that best controls patching frequency while maintaining predictive accuracy.

**Patching Strategies Comparison ($\star$).** To systematically investigate the performance trade-off between the 1-strategy and the $\infty$-strategy, we formulated an evaluation strategy centered on the MAE across varying interval lengths. For this purpose, the PatchTST model, one of the best models from our empirical studies, was trained on the noiseless SynthDS dataset under four distinct policies:

$\mathtt{D}_4$, $\mathtt{D}_8$, $\mathtt{D}_{16}$, and $\mathtt{D}_{32}$. A comparative evaluation of the 1-strategy and $\infty$-strategy was then conducted for each policy. This evaluation was performed on partitions of the codomain of the time-series where the total number of intervals corresponded to a power of two. Figure 7 presents a comparative analysis of the two patching mechanisms where we divided the MAE of the $\infty$-strategy by the MAE of the 1-strategy and we observed the results over different intervals length.

We observe that for smaller intervals where the hypotheses are well-defined and there is no need for averaging, the $\infty$-strategy outperforms the 1-strategy. As the intervals are getting larger, the need for averaging grows, thus making the 1-strategy better.

This analysis shows that for a dataset, when performing inference on small intervals or intervals with clearly defined hypotheses, the $\infty$-strategy is needed, while for larger intervals on which the B-Policy would average, the 1-strategy is needed.

**Decay Rate Analysis ($\nu$).** In the same context as the experiment involving the number of intervals, we conducted an experiment related to the behaviors of the decay rate. We employed the $\mathtt{D}_{32}$ policy and studied decay rates in the set $\{0, 1, 2, 5, \infty\}$. The results of the experiment can be seen in Figure 8.

We observe that the decay rate $\nu$ plays a significant role in enhancing forecasting accuracy, particularly in scenarios where substantial patching is required, i.e., when the interval length is large. In the extreme case where all 32 training intervals are aggregated into a single target interval (resulting in an interval length of 1), the best performance is achieved when $\nu = \infty$, corresponding to a no-decay setting. However, as the intervals of interest become smaller, corresponding to finer-grained target partitions, we observe improved performance when a finite decay rate is applied. In these cases, the decay mechanism effectively introduces a soft overlap between training intervals, promoting smoother generalization across neighboring regions of the domain. This highlights the importance of tuning $\nu$ based on the level of aggregation or granularity used in the target interval structure.

**Interval Separation ($\delta$).** As introduced in Section 3, the `C-Policy` incorporates a hyperparameter, the interval separation $\delta$. In this section, we investigate its effect using the iTransformer model trained on the `SynthDS` trace. Specifically, we vary $\delta$ within the range $[0, 0.4]$ over the domain $\mathcal{X} = [0, 1]$.

Figure 9 illustrates the effect of constraining the sampling space of training intervals by enforcing a minimum separation constraint $\mathcal{I} \geq \delta$. Reducing the sampling space initially yields improved performance; however, beyond a critical threshold $\delta' \approx 5\%$, performance degrades as the model tends to overestimate true interval lengths, thereby introducing bias. It is worth noting that in `SynthDS`, the ground-truth hypotheses are separated by intervals of length $1/4$.